



Significance of surface layer integrity for sustaining the ductility of gradient-structured nickel

Yanfang Liu^a, Yu Zang^a, Yang Cao^{a,*}, Wei Liu^a, Qingzhong Mao^a, Hao Zhou^a, Wei Jiang^a, Yonghao Zhao^a, Yuntian Zhu^{a,b,*}

^a Nano and Heterogeneous Materials Center, School of Materials Science and Engineering, Nanjing University of Science and Technology, Nanjing 210094, China

^b Department of Materials Science and Engineering, City University of Hong Kong, Kowloon, Hong Kong, China

ARTICLE INFO

Keywords:

Gradient structure
Grain refinement
Microstructure
Mechanical properties
Strain hardening

ABSTRACT

Gradient-structured nickel (Ni) was processed by rotationally accelerated shot peening (RASP). The microstructures and mechanical properties of the RASP-processed samples were studied. Nanostructured layers with a thickness of $\sim 50 \mu\text{m}$ were formed on the sample surfaces. Beneath the surface layer there is a transition region in the depth range of $\sim 50\text{--}150 \mu\text{m}$. The transition region contains high densities of dense dislocation walls (DDWs), microbands (MBs), sub-grain boundaries and dislocations, and is susceptible to plastic instability. High-speed RASP processing created some small cracks which deteriorate the integrity of the nanostructured surface layer. During tensile deformation, local stress concentrations are created beneath the surface cracks to trigger plastic instability in the nearby transition region. As a result, interior cracks nucleated and grew in the transition region, and eventually agglomerated with surface cracks to cause premature failure of the bulk material.

1. Introduction

In the last forty years, substantial progress has been made in processing nanostructured metallic materials that usually exhibit superior strength [1,2]. However, due to low strain hardening, nanostructured materials generally show very low ductility [3]. Inspired by the gradient-structured (GS) materials that already exist in nature, such as bamboos, seashells, GS metallic materials consisting of nanostructures and coarse-grained (CG) structures have recently been developed. The proper design of gradient structures grants materials with both high strength and high ductility beyond the empirical prediction [4,5]. It is noted that gradient structure is regarded as one type of heterostructures that have been found to produce superior mechanical properties [6].

In order to process GS materials, some surface nano-crystallization (SNC) techniques have been developed [7], such as surface mechanical attrition treatment (SMAT) [8,9], surface mechanical grinding treatment (SMGT) [4], surface mechanical rolling treatment (SMRT) [10] and rotationally accelerated shot peening (RASP) [11,12]. All the SNC techniques share one basic concept – the severe plastic deformation (SPD) imposed shear strain transmits and decays from the surface towards the interior, resulting in gradient structures and varied properties

in the metallic material. Hence, the gradient structures are affected by intrinsic factors, such as crystalline structure, stacking fault energy (SFE), grain size, and extrinsic factors, such as strain, strain rate and temperature [2,13,14].

The gradient structures and the mechanical properties of the GS metallic materials are versatile and easily adjustable. It has been widely reported that mechanical behaviors of GS materials are different from that of the corresponding homogeneous materials [4,5,12,14]. High strain incompatibility between the high strength surface layer and the soft core is accommodated by defused shear bands in the surface layer [15,16] and a high density of geometrically necessary dislocations (GNDs) in the soft core [17,18]. As a result, improved strength, sustained ductility and even an evident upturn of strain hardening rate can be realized during the tensile deformation [18]. It was recently conceptualized that the high flow stress in GS materials is attributed to hetero-deformation induced (HDI) stress and the upturn of strain hardening rate is the mechanical response of the HDI hardening effect [6,19].

In despite of the encouraging progresses in both the development and research of GS materials, it is also noticed that the superior mechanical properties in GS materials are not guaranteed. There must be

* Corresponding author at: Nano and Heterogeneous Materials Center, School of Materials Science and Engineering, Nanjing University of Science and Technology, Nanjing 210094, China (Y. Zhu).

E-mail addresses: y.cao@njtu.edu.cn (Y. Cao), y.zhu@cityu.edu.hk (Y. Zhu).

<https://doi.org/10.1016/j.matlet.2021.130491>

Received 14 June 2021; Accepted 17 July 2021

Available online 20 July 2021

0167-577X/© 2021 Elsevier B.V. All rights reserved.

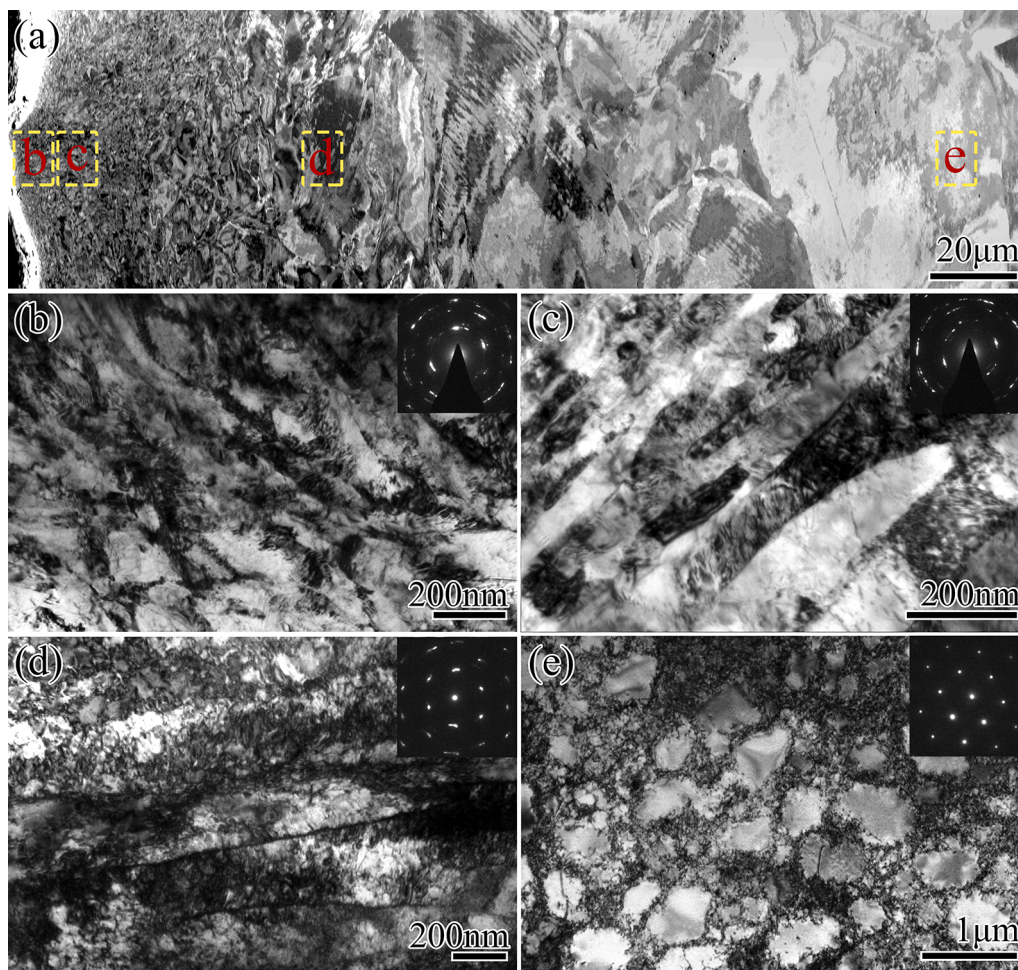


Fig. 1. Microstructures observed in the 1.6 mm-5 min-RASP sample. (a) A SEM image showing gradient structure from the surface to the $\sim 220 \mu\text{m}$ depth; TEM images showing microstructures at the depths of (b) $\sim 2 \mu\text{m}$ (area b), (c) $\sim 5 \mu\text{m}$ (area c), (d) $\sim 60 \mu\text{m}$ (area d) and (e) $\sim 200 \mu\text{m}$ (area e), respectively.

some other factors affecting the mechanical behaviors of GS materials. In this work, the microstructures and tensile properties of a representative GS Ni is studied in depth. The evolution of local microhardness (local strength) during tensile deformation is analyzed in detail. The significance of surface layer integrity for effective HDI strengthening effect is unambiguously revealed.

2. Material and methods

A commercial purity nickel (Ni, 99.3 wt%) was chosen as the model material. The as-received model material has equiaxed coarse grains with an average size of $\sim 120 \mu\text{m}$. RASP was conducted, at room temperature by using GCr15 bearing steel balls with a diameter of 1 mm and a velocity of 70 m/s, to process Ni sample plates with gradient structures on both sides. The first sample with dimensions of $50 \text{ mm} \times 25 \text{ mm} \times 1.6 \text{ mm}$ was RASP processed for 5 mins, and named 1.6 mm-5 min-RASP sample hereafter. The second sample with dimensions of $50 \text{ mm} \times 25 \text{ mm} \times 2.4 \text{ mm}$ was RASP processed for 5 mins, and named 2.4 mm-5 min-RASP sample hereafter. An as-received sample is used as the reference material, and named CG sample hereafter.

The samples were analyzed by using Zeiss Auriga scanning electron microscope (SEM) and TECNAI-G2-20-LaB6 transmission electron microscope (TEM). The specimens for SEM and TEM analysis were prepared by the standard methods which can be found in the literature [20]. Hardness tests were conducted on the polished cross-sections of the samples, by an HMV-G21 Vickers hardness tester with a load of 980.7 mN and the dwell time of 15 s. The tensile tests were performed at

room temperature, using an AGS-X10KN tensile testing machine operating at a constant strain rate of $1.6 \times 10^{-3} \text{ s}^{-1}$.

3. Results and discussion

Fig. 1a is a SEM image showing the gradient structure in the 1.6 mm-5 min-RASP sample. Since secondary electron signals are captured for SEM imaging, the contrast is associated with the variation of local microscopic strain. Frequent change in contrast at the very surface indicates frequent variation of local strain gradients which in turn suggests high densities of dislocations in the local area. With increasing depth beneath the surface, high contrast and low contrast areas both become larger and intact, indicating that dislocations are spread out and dislocation densities are lowered. A large fraction of these dislocations are GNDs, as confirmed by both EBSD Kernel average misorientation (KAM) analysis, TEM observation and early literatures [12,13,18].

Fig. 1b shows ultrafine grains with blurred GBs and high densities of dislocations at the depth of $\sim 2 \mu\text{m}$ beneath the surface. The selected area diffraction (SAED) pattern inset in **Fig. 1b** shows both diffraction spots and arcs, suggesting the presence of both high angle and low angle GBs in the local area. At the depth of $\sim 5 \mu\text{m}$ beneath the surface, elongated grains with high angle GBs are formed, and the average grain width is $\sim 58 \text{ nm}$, as shown in **Fig. 1c**. At the depth of $\sim 60 \mu\text{m}$, a high density of dislocations enables the formation of DDWs and MBs [2], as shown in **Fig. 1d**. The SAED pattern inset contains two sets of diffraction arcs. The arcs tend to separate into bright spots, indicating that some DDWs may have transformed into sub-grain boundaries. **Fig. 1e** shows

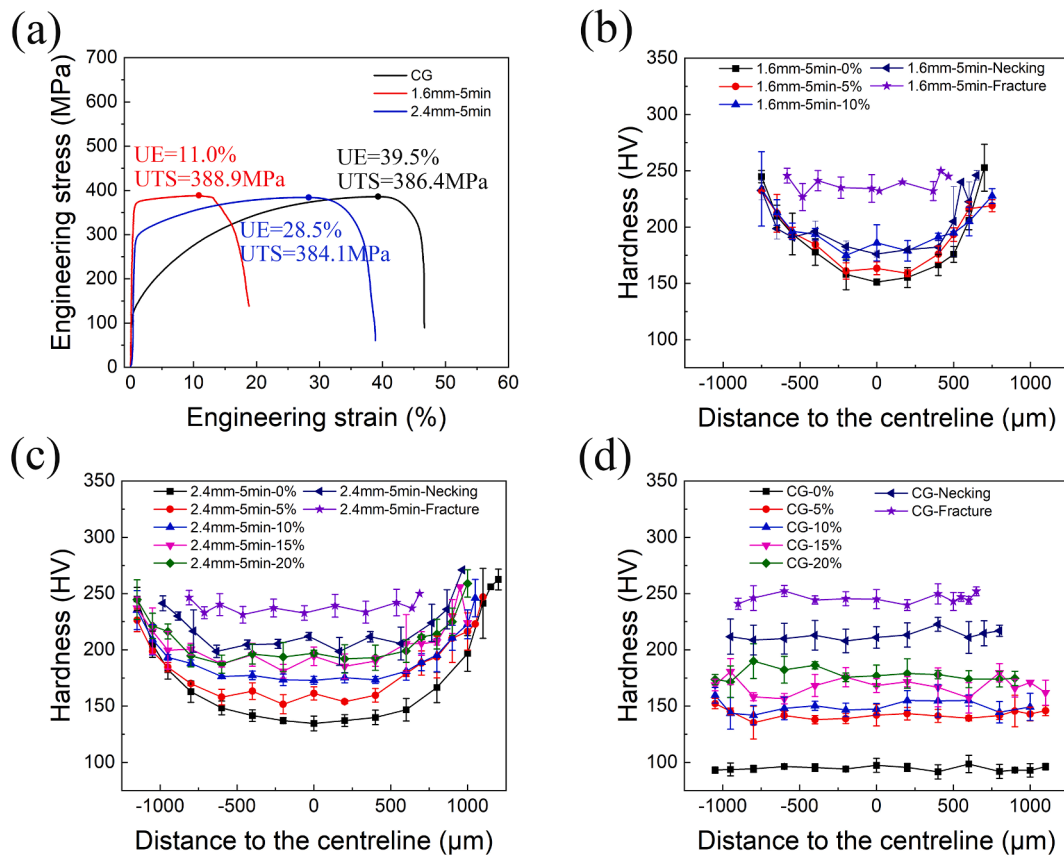


Fig. 2. Mechanical properties measured from the 1.6 mm-5 min-RASP, 2.4 mm-5 min-RASP and CG samples. (a) Engineering stress–strain curves. Hardness distributions from the surfaces to the centerlines of the (b) 1.6 mm-5 min-RASP sample, (c) 2.4 mm-5 min-RASP sample and (d) the homogeneous CG sample.

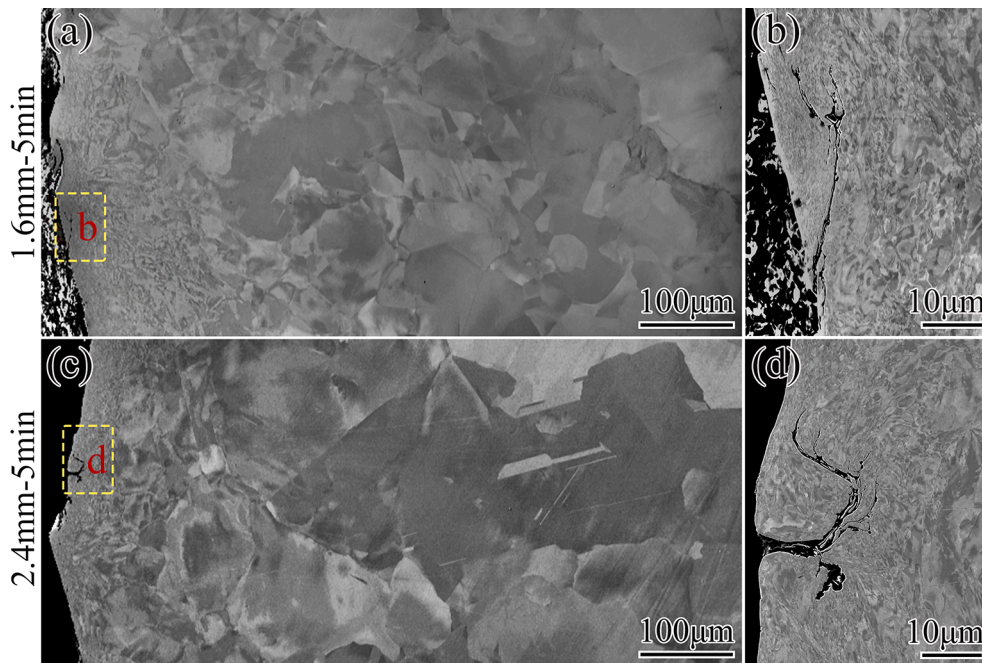


Fig. 3. SEM images showing gradient structures of RASP samples before the tensile test. (a) 1.6 mm-5 min-RASP sample, (b) the magnified image of the truncated area b in (a); (c) 2.4 mm-5 min-RASP sample, (d) the magnified image of the truncated area d in (c).

equiaxed dislocation cells with an average cell size of ~500 nm at the depth of ~200 μm. The dislocations are mostly located at the cell walls and only a few dislocations are randomly scattered in cell interiors.

As shown in Fig. 2a, the yield strength (YS) of the 1.6 mm-5 min-RASP, 2.4 mm-5 min-RASP and CG samples are 357.7 MPa, 279.6 MPa and 125.9 MPa, respectively; The uniform elongation (UE) of the 1.6

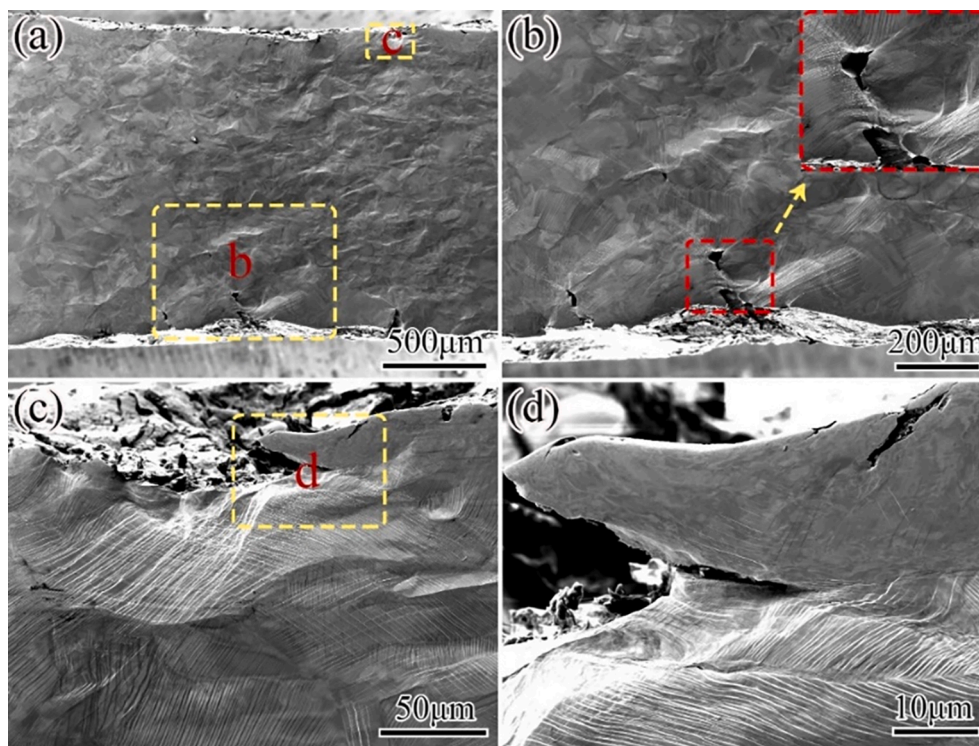


Fig. 4. SEM images showing the topography on the cross-sectional surface of the 1.6 mm-5 min-RASP sample at necking. (a) A low magnification image of the necking region; (b) a magnified image of the area b in (a); (c) a magnified image of the area c in (a); (d) a magnified image showing a surface crack in the truncated area d in (c).

mm-5 min-RASP, 2.4 mm-5 min-RASP and CG samples are 11.0%, 28.5% and 39.5%, respectively. RASP processing has improved the YS of the Ni samples at the expense of ductility. However, the ultimate tensile strength (UTS) of the three samples are very similar at about 385 MPa.

Hardness distributions through the depths are shown for the 1.6 mm-5 min-RASP, 2.4 mm-5 min-RASP and CG samples deformed to pre-determined elongation values in Fig. 2b-d. The hardness data points are located with reference to the longitudinal centerline on the cross-section of the tensile sample. Thus, position 0 on the x-axis is the core region where that hardness is the lowest for the 1.6 mm-5 min-RASP, 2.4 mm-5 min-RASP samples when tensile strain is 0%, as shown in Fig. 2b and c. As the tensile strain increases, the hardness at the core region is gradually increased to be comparable to that at the sample surface, and the hardness at the surface is almost unchanged. Provided that hardness is directly proportional to strength, strain hardening evidently occurred beneath the surface. The hardness values on the cross sections of the fractured 1.6 mm-5 min-RASP, 2.4 mm-5 min-RASP and CG samples are nearly identical, depicted by the pink star data points in Fig. 2b-d, suggesting that the upper limit of strain hardening in the core region of the GS sample is comparable to the CG sample.

The 1.6 mm-5 min-RASP and 2.4 mm-5 min-RASP samples have very similar gradient structures at the surfaces, as shown in Fig. 3. In both samples, the severely deformed surface layers are about 50 μm in thickness, as shown in Fig. 3a and c. Some cracks extend more than ~ 10 μm beneath the surface, breaking the integrity of the nanostructured surface layers. When the 1.6 mm-5 min-RASP sample was tensile deformed to necking, some cracks formed at ~ 100 μm beneath the surface as shown in Fig. 4a and b. As shown in Fig. 4b, an interior crack tends to merge with the pre-existing surface crack. Fig. 4c shows partial exfoliation on the surface with a width of ~ 120 μm , leaving an arch-shaped crack extending in the direction nearly parallel to the loading axis. Since the pre-existing surface cracks tend to cause exfoliation instead of extending deeply towards the interior, surface cracks are not the sole contributor to the limited strain hardening capacity, premature

failure and thus low ductility of the RASP samples.

Based on SEM observations of several tensile deformed 1.6 mm-5 min-RASP and 2.4 mm-5 min-RASP samples, it is confirmed that interior cracks occurred at the depth of ~ 50 – 150 μm beneath the surface. According to Fig. 1d, DDWs, MBs, sub-grain boundaries and high-density dislocations are found in this depth range. This depth range is the transition region from nanostructured surface layer to the CG core, as shown in Fig. 1c-e and Fig. 3. The microstructural features in the transition region match exactly with the microstructures observed in the compressive residual stress (CRS) layer of the GS interstitial free steel [21]. According to literatures [12,18,21,22], the transition region experiences a high CRS during the early stage of strain hardening. While the regions adjacent to the transition region all experience tensile residual stresses, microscopic strain gradients are created at the border of the transition region. In accommodation to the local strain gradients, high densities of GNDs are concentrated at the transition region. As a result, the highest strain incompatibility and most strain hardening should exist at the transition region [21]. As such, whether the transition region can sustain a high density of GNDs and thus to accommodate the strain incompatibility, is critically important for achieving high strength and high ductility. However, high densities of pre-existing dislocation structures limit the GND generation rates in the transition region, and thus the transition region is sensitive to stress concentration and plastic instability. It has been proven that high strength nanostructured surface layer can prevent crack initiation, and ductile CG core can suppress crack propagation [9,23]. Thus, high strength nanostructured surface layers with integrity is critically needed to constrain the less stable transition region. In the current case, several cracks on the surface layer deteriorate the integrity, and meanwhile create local stress concentrations which may trigger plastic instability in the transition region. Once the crack nucleated in the transition region, it expands towards the preexisting crack on nanostructured surface layer, resulting in premature failure of the GS material.

4. Conclusions

A CG Ni sample was processed by RASP to produce GS Ni materials. Microstructures and mechanical properties of the RASP samples and CG samples are analyzed and compared. Both TEM and hardness tests reveal that the RASP imposed shear strain penetrate all the way to the cores of both the 1.6 mm-5 min-RASP, 2.4 mm-5 min-RASP samples. However, nanostructured surface layers are only $\sim 50\ \mu\text{m}$ in thickness. At the depth of $\sim 50\text{--}150\ \mu\text{m}$ beneath the surface is the transition region featuring DDWs, MBs, sub-grain boundaries and high-density dislocations. During tensile loading, the transition region experiences very high strain incompatibility due to strain partitioning between the hard surface layers and ductile inner core. As a combined result of high densities of dislocation structures and high strain incompatibility, the transition region is susceptible to plastic instability. The nanostructured surface layer with excellent integrity can help constraining the adjacent transition region to delay strain localization and crack initiation. However, pre-existing cracks created during RASP processing deteriorate surface layer integrity. As a result, local stress concentrations are created under the pre-existing cracks to trigger the plastic instability in the transition region underneath, causing interior cracks and premature failure of the bulk material.

Declaration of Competing Interest

The authors declare that they have no known competing financial interests or personal relationships that could have appeared to influence the work reported in this paper.

Acknowledgements

This work is supported by the National Natural Science Foundation of China (Grant No. 51931003, 52071181 and 51971112) and the Fundamental Research for the Central Universities (No. 30919011405). The authors are thankful for the technical support from Jiangsu Key Laboratory of Advanced Micro & Nano Materials and Technology, and the Materials Characterization Facility of Nanjing University of Science and Technology.

References

- [1] A.P. Zhilyaev, T.G. Langdon, Using high-pressure torsion for metal processing: Fundamentals and applications, *Prog. Mater. Sci.* 53 (6) (2008) 893–979.
- [2] Y. Cao, S. Ni, X. Liao, M. Song, Y. Zhu, Structural evolutions of metallic materials processed by severe plastic deformation, *Mater. Sci. Eng. R* 133 (2018) 1–59.

- [3] I.A. Ovid'ko, R.Z. Valiev, Y.T. Zhu, Review on superior strength and enhanced ductility of metallic nanomaterials, *Prog. Mater. Sci.* 94 (2018) 462–540.
- [4] T.H. Fang, W.L. Li, N.R. Tao, K. Lu, Revealing Extraordinary Intrinsic Tensile Plasticity in Gradient Nano-Grained Copper, *Science* 331 (6024) (2011) 1587–1590.
- [5] X.L. Wu, M.X. Yang, F.P. Yuan, L. Chen, Y.T. Zhu, Combining gradient structure and TRIP effect to produce austenite stainless steel with high strength and ductility, *Acta Mater.* 112 (2016) 337–346.
- [6] Y. Zhu, K. Ameyama, P.M. Anderson, L.J. Beyerlein, H. Gao, H.S. Kim, E. Lavernia, S. Mathaudhu, H. Mughrabi, R.O. Ritchie, N. Tsuji, X. Zhang, X. Wu, Heterostructured materials: superior properties from hetero-zone interaction, *Mater. Res. Lett.* 9 (1) (2021) 1–31.
- [7] K. Lu, J. Lu, Surface Nanocrystallization (SNC) of Metallic Materials-Presentation of the Concept behind a New Approach, *J. Mater. Sci. Technol.* 15 (03) (1999) 193–197.
- [8] K. Lu, J. Lu, Nanostructured surface layer on metallic materials induced by surface mechanical attrition treatment, *Mater. Sci. Eng. A* 375-377 (2004) 38–45.
- [9] K.Y. Zhu, A. Vassel, F. Brisset, K. Lu, J. Lu, Nanostructure formation mechanism of α -titanium using SMAT, *Acta Mater.* 52 (14) (2004) 4101–4110.
- [10] H.W. Huang, Z.B. Wang, J. Lu, K. Lu, Fatigue behaviors of AISI 316L stainless steel with a gradient nanostructured surface layer, *Acta Mater.* 87 (2015) 150–160.
- [11] X. Wang, Y.S. Li, Q. Zhang, Y.H. Zhao, Y.T. Zhu, Gradient Structured Copper by Rotationally Accelerated Shot Peening, *J. Mater. Sci. Technol.* 33 (7) (2017) 758–761.
- [12] Y. Liu, Y. Cao, H. Zhou, X. Chen, Y. Liu, L. Xiao, X. Huan, Y. Zhao, Y. Zhu, Mechanical Properties and Microstructures of Commercial-Purity Aluminum Processed by Rotational Accelerated Shot Peening Plus Cold Rolling, *Adv. Eng. Mater.* 22 (1) (2020) 1900478, <https://doi.org/10.1002/adem.201900478>.
- [13] J. Zhang, Y. Cao, H. Gao, X.u. Yang, B. Shu, Y. Zhu, B. Sharma, K. Ameyama, X. Zhu, Influence of Strain Rate on Mechanical Behaviours of Gradient-Structured Copper, *Mater. Trans.* 61 (4) (2020) 708–717.
- [14] M.N. Hasan, Y.F. Liu, X.H. An, J. Gu, M. Song, Y. Cao, Y.S. Li, Y.T. Zhu, X.Z. Liao, Simultaneously enhancing strength and ductility of a high-entropy alloy via gradient hierarchical microstructures, *Int. J. Plast.* 123 (2019) 178–195.
- [15] Y. Wang, C. Huang, Y. Li, F. Guo, Q. He, M. Wang, X. Wu, R.O. Scattergood, Y. Zhu, Dense dispersed shear bands in gradient-structured Ni, *Int. J. Plast.* 124 (2020) 186–198.
- [16] F. Yuan, D. Yan, J. Sun, L. Zhou, Y. Zhu, X. Wu, Ductility by shear band delocalization in the nano-layer of gradient structure, *Mater. Res. Lett.* 7 (1) (2019) 12–17.
- [17] M. Yang, Y. Pan, F. Yuan, Y. Zhu, X. Wu, Back stress strengthening and strain hardening in gradient structure, *Mater. Res. Lett.* 4 (3) (2016) 145–151.
- [18] X. Wu, P. Jiang, L. Chen, F. Yuan, Y.T. Zhu, Extraordinary strain hardening by gradient structure, *Proc. Natl. Acad. Sci.* 111 (20) (2014) 7197–7201.
- [19] Y. Zhu, X. Wu, Perspective on hetero-deformation induced (HDI) hardening and back stress, *Mater. Res. Lett.* 7 (10) (2019) 393–398.
- [20] Y. Liu, Y. Cao, Q. Mao, H. Zhou, Y. Zhao, W. Jiang, Y. Liu, J.T. Wang, Z. You, Y. Zhu, Critical microstructures and defects in heterostructured materials and their effects on mechanical properties, *Acta Mater.* 189 (2020) 129–144.
- [21] M.-X. Yang, R.-G. Li, P. Jiang, F.-P. Yuan, Y.-D. Wang, Y.-T. Zhu, X.-L. Wu, Residual stress provides significant strengthening and ductility in gradient structured materials, *Mater. Res. Lett.* 7 (11) (2019) 433–438.
- [22] X. Wu, Y. Zhu, Heterogeneous materials: a new class of materials with unprecedented mechanical properties, *Mater. Res. Lett.* 5 (8) (2017) 527–532.
- [23] T.H. Fang, N.R. Tao, K. Lu, Tension-induced softening and hardening in gradient nanogained surface layer in copper, *Scr. Mater.* 77 (2014) 17–20.